REVISTA Mundi
Engenharia, Tecnologia e Gestão
INSTITUTO FEDERAL

A PERFORMANCE COMPARISON OF DISCRETE-TIME LEAST SQUARES-BASED ROBUST MODEL REFERENCE ADAPTIVE CONTROL APPROACHES APPLIED ON GRID-SIDE CURRENT CONTROL OF GRID-TIED POWER CONVERTERS BY LCL FILTER

UMA COMPARAÇÃO DE DESEMPENHO DE CONTROLADORES ROBUSTO ADAPTATIVOS POR MODELO DE REFERÊNCIA DISCRETOS NO TEMPO BASEADOS EM MÍNIMOS QUADRADOS APLICADOS AO CONTROLE DE CORRENTE DO LADO DA REDE DE CONVERSORES DE POTÊNCIA CONECTADOS A REDE POR FILTRO LCL

Paulo Jefferson Dias de Oliveira Evald[1]

Abstract: In this work, two Robust Model Reference Adaptive Controllers (RMRAC) for grid-side current control of a static 3-wire converter with LCL filter are implemented and compared. The adaptation law used to adjust gains online is a modified Least Square (LS) algorithm. In both methods there is no need using resonant controllers to reject exogenous disturbance. Thereby, it is presented, step-by-step, how to implement both strategies, pointing out benefits and drawbacks of each technique and comparing their performance to track model reference output and robustness to deal with parametric variation of grid conditions. The performance comparison parameters considered are: THD (Total Harmonics Distortion), mean of absolute tracking error and maximum overshoot. Simulation results are presented to support the discussion.

***Keywords*:** Robust adaptive control. Grid-tied converter. LCL filter.

Resumo: Neste trabalho, dois controladores robustos adaptativos por modelo de referência para o controle de corrente de um conversor estático a três fios com filtro LCL são implementados e comparados. A lei de adaptação usada para ajustar os ganhos online é um algoritmo dos mínimos quadrados modificado. Em ambos os métodos não há necessidade de utilizar controladores ressonantes para rejeitar distúrbios exógenos. Assim, é apresentado, passo a passo, como implementar ambas as estratégias, apontando vantagens e desvantagens de cada técnica e comparando seu desempenho para rastrear a saída do modelo de referência e robustez para lidar com variações paramétricas da rede elétrica. Os parâmetros usados na comparação de performance são: distorção harmônica total, média do erro de rastreamento absoluto e máximo sobressinal. Resultados de simulação são apresentados para sustentar a discussão.

Palavras-chave: Controle robusto adaptativo. Conversor conectado a rede. Filtro LCL.

[1]Doutor, Universidade Franciscana, paulo.evald@gmail.com.

1 Introduction

In recent years, renewable energy systems are receiving more and more attention due to the global concerning about natural resources shortage and environmentally sustainability politics. Thereby, nuclear and thermal power plants have been replaced by wind and solar farms, once they do not use fossil fuels for electricity generation (NOURELDEEN; HAMDAN, 2018; BROEER et al., 2018; BROUWER et al., 2015). Moreover, these clean energy systems are interesting alternative to the hydroelectric plant, because they present reduced ecological impact on local ecosystems (FEARNSIDE, 2011; AMARAL; LIMA; GUEDES, 2017; BRITO; AGUIAR, 2019).

On renewable energy generation systems, the grid-tied converter, generally modulated voltage-source converters (KANTAR; HAVA, 2016; ZHANG et al., 2016), are commonly associated to LCL filter to realise dc to ac power conversion (XU; XIE; TANG, 2013; GUAN et al., 2018). The LCL filter presents advantages in face to L filter, due to its reduced structure that is composed by smaller reactive components (ZHAO; CHEN, 2009), which consume less reactive power, besides has the ability to attenuate the high-frequency current harmonics (HAN et al., 2017; LIMA et al., 2018), achieved thanks to power electronic technologies development (FARAKHOR; ABAPOUR; SABAHI, 2018).

However, when it is used the LCL filter on renewable energy system, the grid-injected currents can be easily distorted (XIN et al., 2017). Thereby, it is fundamental a reliable current control loop to ensure energy quality. In this point there are a considerable range of controllers to deal with currents regulation, such as: PI controller (KIPKE; CHHOR; SOURKOUNIS, 2018), PI with Resonant controller (MAHMUD; RAHMAN, 2018), Deadbeat controller (HE et al., 2016), Repetitive controller (GAO et al., 2018), Internal Model-based controller (LEITNER et al., 2018), Optimal controller (HUERTA et al., 2011), Robust controller (BENRABAH; XU; GAO, 2018), Sliding Mode controller (VIEIRA et al., 2017), Predictive controller (BOSCH; STAIGER; STEINHART, 2017), among other techniques. Although these techniques present excellent performance, when properly designed, they only ensure this high level of performance when grid does not vary its impedance relevantly. It occur due to fixed-gains nature of these controllers, which has limited operation range that do not guarantee good performance against unmodelled dynamics or parametric variations outside it (FLORA; GRÜNDLING, 2008).

As alternative, adaptive controllers have been proposed to due with grid impedance variation and variable operation points. Some interesting techniques were

proposed on (MASSING; PINHEIRO, 2010; MASSING et al., 2011; TAMBARA et al., 2013; TAMBARA et al., 2017; SILVEIRA et al., 2016), which are based on RMRAC (Robust Model Reference Adaptive Control). These approaches, besides dealing well with variable operating point, unmodelled dynamics and parametric variations, also reject exogenous disturbances without need conventional Proportional-Resonant Controllers, which are often used.

The direct RMRAC methods are divided by two approaches: state feedback and output feedback. In light to analyse advantages and drawbacks of each method, in this work it is presented a performance comparison of both methods, applied on grid-injected currents control of a three-phase 3-wire power converter connected to the grid with an LCL filter. The analysis consists in evaluate mean of absolute tracking error, maximum overshoot and THD (Total Harmonics Distortion) due converter switching, starting from same conditions and with same adaptive law, a modified Least Square (LS) algorithm. Simulation results are presented, taking into account real plant parameters, converter modulation, implementation delay and parametric variation of grid impedance, from strong to weak grid.

The regarding of this work is given as follows: Section II shows briefly the grid-tied converter and Section III gives the mathematical background of RMRAC methods. Next, Section IV presents simulation results and a discussion about controllers performance. Finally, Section V gives our conclusions.

2 Mathematical Model of Grid-Tied Converter by LCL filter

The mathematical modelling of grid-tied 3-wire power converters with LCL filters is well discussed on aforementioned works, they are (MASSING; PINHEIRO, 2010; MASSING et al., 2011; TAMBARA et al., 2013; TAMBARA et al., 2017) and others. Then, here, the model will be briefly presented.

To simulate the grid-tied power converter with LCL filter, the following system components were taken into account: the clean energy source is simulated as a continuous voltage source V_d, the converter switches are considered ideal, the grid is assumed to be predominantly inductive, modelled by a sinusoidal source V_s in series with an inductance L_{g2} and parasitic resistance R_{g2} and the LCL filter. Here, the equivalent LCL circuit is represented by the Thevenin equivalent in relation to the PCC (Point of Common Coupling), as (TAMBARA et al., 2017). It is compounded by converter-side inductors L_c, with associated parasitic resistance R_c, a bank of

capacitors C and grid-side inductors L_{g1}, with associated parasitic resistance R_{g1}. The total grid-side inductance and resistance are given by $L_g = L_{g1}+L_{g2}$ and $R_g = R_{g1}+R_{g2}$, respectively.

It is highlighted that three-phase LCL model in three-phase coordinates (commonly named abc or rst coordinates) are complex to design a controller, once it is coupled (EVALD et al., 2021a). Therefore, it is usually converted to two identical decoupled single-phase linear invariant-time systems (named $\alpha\beta$ coordinates), through Clarke Transform (DUESTERHOEFT; SCHULZ; CLARKE, 1951). To apply the fixed-gains controllers there is necessary to transform these synchronous frame in an stationary frame, which results on dq coordinates. However, for adaptive controller this step is not need, reducing the computational burden for processing it on microcontrollers. Then, considering converter disconnected from the grid, the transfer function of decoupled system $G(s)$ is

$$G(s) = \frac{i_g(s)}{u(s)} = \frac{\dfrac{1}{L_g L_c C}}{s^3 + \dfrac{(R_g L_c + R_c L_g)}{L_g L_c} s^2 + \dfrac{(L_c + L_g + R_g R_c C)}{L_g L_c C} s + \dfrac{R_g + R_c}{L_g L_c C}} \tag{1}$$

where $i_g(s)$ and $u(s)$ are grid-injected currents and voltage synthesised by converter through modulation technique. Moreover, considering equilibrated phases, there is no path for current conduction on the 0 axis, then, it can be disregarded (EVALD; TAMBARA; GRÜNDLING, 2020). Finally, for approaching to physical system, implementation delay was considered in the simulation by executing $u(k) = u(k-1)$.

3 Mathematical Background of RMRAC and Adaptive Law

In light of elucidation, in this Section, a step-by-step of discrete-time LS-based RMRAC theory for SISO (Single Input Single Output) plants is provided, with aim to facilitate comprehension for anyone who want to start working with robust adaptive controllers. The general theory is identical for both approaches: state feedback and output feedback, then the reader can follows securely the steps to implementation for both, taking attention in the filters structure, where they differ each other. First of all, assuming that continuous-time plant was properly discretised, a discrete-time SISO plant $G(z)$ can be described as follows,

$$G(z) = G_0(z)[1 + \mu\Delta_m(z)] + \mu\Delta_a(z), \tag{2}$$

where $\Delta_a(z)$ and $\Delta_m(z)$ are an additive and a multiplicative dynamics.Moreover, μ is a positive constant that, with no loss of generality can be equal for both dynamics (EVALD et al., 2021b). Besides, $G_0(z)$ is the known (or modelled) part of the plant, given by

$$G_0(z) = k_p \frac{Z_p(z)}{R_p(z)}, \tag{3}$$

where $Z_p(z)$ and $R_p(z)$ are monic polynomials of degree m and n, respectively, it means $m < n$. Also, k_p is the high frequency gain of the known part of plant.

The modelled part of the plant and additive/multiplicative dynamics have to satisfy the following assumptions (IOANNOU; SUN, 2012):
A1) $Z_p(z)$ is a Schur polynomial, it means that all roots of $Z_p(z)$ are inside the unit radius circle of Z plan;
A2) The high frequency gain k_p signal is know;
A3) $\Delta_a(z)$ is a strictly proper Schur transfer function;
A4) $\Delta_m(z)$ is a Schur transfer function;
A5) The upper bound on stability margin of $\Delta_a(z)$ and $\Delta_m(z)$ are know and stable.

The reference model is designed with the same order and relative degree of $G_0(z)$, as follows.

$$y_m = W_m(z)r = k_m \frac{Z_m(z)}{R_m(z)} r, \tag{4}$$

where $Z_m(z)$ and $R_m(z)$ are monic Schur polynomials with degree m^* and n^*, respectively. As well as k_p, k_m is also the high frequency gain, but of reference model. In addition, $r(k)$ is a limited reference signal. The reference model has to satisfy only one assumption, which is:
B1) $R_m(z)$ is an arbitrary Schur monic polynomial of relative degree $n^* = n - m > 0$.

The control action $u(k)$ is given by $u(k) = \boldsymbol{\theta}^T(k)\boldsymbol{\omega}(k)$, where $\boldsymbol{\theta}(k)$ is the adaptive gains vector and $\boldsymbol{\omega}(k)$ is a vector formed by internal filters, plant output, reference signal and disturbance rejection terms. In this point is where both approaches differ each other. For output feedback approach, the $\boldsymbol{\omega}(k)$ consists in the following structure:

$$\boldsymbol{\omega}^T(k) = [\ \boldsymbol{\omega}_1^T(k)\ \boldsymbol{\omega}_2^T(k)\ y(k)\ r(k)\ V_s(k)\ V_c(k)\ ], \tag{5}$$

where $\boldsymbol{\omega}_1(k)$ and $\boldsymbol{\omega}_2(k)$ are reconstructive filters, $y(k)$ is plant output, $V_s(k)$ and $V_c(k)$ are phase and quadrature components of exogenous disturbance.

The reconstructive filters have dimension $(n-1) \times (n-1)$ and are formed as

$$\begin{aligned} \boldsymbol{\omega}_1(k+1) &= (\boldsymbol{I} + \boldsymbol{F}T_s)\boldsymbol{\omega}_1(k) + \boldsymbol{q}T_s u(k), \\ \boldsymbol{\omega}_2(k+1) &= (\boldsymbol{I} + \boldsymbol{F}T_s)\boldsymbol{\omega}_2(k) + \boldsymbol{q}T_s y(k), \end{aligned} \tag{6}$$

where $\boldsymbol{I}$ is an identity matrix, T_s is the sampling time, and $(\boldsymbol{F}, \boldsymbol{q})$ is a controllable pair with a stable matrix $\boldsymbol{F}$ and a vector of controllable parameters $\boldsymbol{q}$, with dimensions $n-1 \times n-1$ and $n-1$, respectively (IOANNOU; TSAKALIS, 1986).

On other way, for state feedback approach, instead of reconstructive, the states themselves are used to fed back the control loop. As the plant output is always a state, it has not to be included twofold as a state, once $y(k)$ is already one of dynamics which compound $\boldsymbol{\omega}(k)$ vector. It reduces the quantity of computations and simplify the control design. However, when implemented experimentally, it will require more sensors than output feedback approach.

For gains adaptation, a Least Square algorithm was utilised (IOANNOU; SUN, 2012),

$$\boldsymbol{\theta}(k+1) = \boldsymbol{\theta}(k) - T_s\sigma(k)\boldsymbol{P}(k)\boldsymbol{\theta}(k) - T_s\kappa\boldsymbol{P}(k)\frac{\boldsymbol{\zeta}(k)\epsilon(k)}{m^2(k)}, \tag{7}$$

where $\boldsymbol{P}(k)$ is the covariance matrix, κ is a positive parameter and ϵ is the augmented error, given as follows

$$\epsilon(k) = e_1(k) + \boldsymbol{\theta}^T(k)\boldsymbol{\zeta}(k) - \nu(k), \tag{8}$$

where ν is the control signal filtered by reference model ($\nu = W_m(z)u$) and $\boldsymbol{\zeta}(k)$ is the $\boldsymbol{\omega}(k)$ filtered by reference model ($\boldsymbol{\zeta} = W_m(z)\boldsymbol{\omega}$). In addition, the tracking error $e_1(k)$ is given by difference between model reference output and plant output ($e_1(k) = y_m(k) - y(k)$).

The covariance matrix $\boldsymbol{P}(k)$ defines the parametric convergence. It can be calculated from different forms. In this work the following algorithm is used:

$$\boldsymbol{P}(k+1) = \boldsymbol{P}(k) - T_s\boldsymbol{P}(k)\boldsymbol{\zeta}(k)\boldsymbol{\zeta}^T(k)\boldsymbol{P}(k) + T_s\beta\boldsymbol{\iota} \tag{9}$$

where $\boldsymbol{\iota}$ is a matrix of ones. It is highlighted that term $T_s\beta\boldsymbol{\iota}$ is used to avoid $\boldsymbol{P}$ stagnate in zero.

The σ-modification is one of projection methods that can be used to contribute to the robustness of adaptive controller. Moreover, it avoids parameters drifting and is

calculated as

$$\sigma(k) = \begin{cases} 0 & \text{if} \quad \|\boldsymbol{\theta}(k)\| < M_0 \\ \sigma_0(\frac{\|\boldsymbol{\theta}(k)\|}{M_0} - 1) & \text{if} \quad M_0 \leq \|\boldsymbol{\theta}(k)\| < 2M_0, \\ \sigma_0 & \text{if} \quad \|\boldsymbol{\theta}(k)\| \geq 2M_0 \end{cases} \tag{10}$$

where $M_0 > \|\boldsymbol{\theta}^*\|$ is the upper limit of $\boldsymbol{\theta}(k)$ norm, which can be securely oversized due to lack of knowledge of $\|\boldsymbol{\theta}(k)^*\|$ and σ_0 is the maximum value of the modification function (EVALD; TAMBARA; GRÜNDLING, 2020).

Besides, the normaliser $m^2(k)$ also contributes for robustness of adaptive controller (EVALD; TAMBARA; GRÜNDLING, 2020), and can be modified as project's needs. It is calculated as follows,

$$m^2(k) = 1 + \boldsymbol{\zeta}^T(k)\boldsymbol{\zeta}(k). \tag{11}$$

4 Simulation Results

The simulations include converter switching dynamics, governed by SVM (Space Vector Modulation) (PINHEIRO et al., 2005), to synthesise control action. In addition, the controller was synchronised with the grid by Kalman Filter (CARDOSO et al., 2008), thereby, while it is not synchronised, it remains inhibited. The signals extracted from grid are its phase and quadrature, used in the disturbance rejection control term and to generate current references for reference models. Then, in this proposed control strategy, it is fundamental use both algorithms, the controller itself and Kalman filter. The grid frequency, line voltage range and DC bus voltage were set to 60 Hz, 110 V and 400 V, respectively. In addition, converter's switching frequency and controller's sampling frequency were both 5 kHz. The parameters of LCL filter and grid are shown on Table 1.

Table 1: Grid and LCL filter parameters

Symbol	Parameter	Value
L_c	Converter-side inductance	1 mH
R_c	Converter-side resistance	50 mΩ
C	Capacitance of LCL filter	62 μF
L_{g1}	Grid-side inductance	0.3 mH
R_{g1}	Grid-side resistance	50 mΩ
L_{g2}	Grid inductance	0.5 mH
R_{g2}	Grid resistance	50 mΩ

Source: From author (2021)

With the parameters from Table 1, by replacing them on (1), the resulting transfer function is obtained,

$$G(s) = \frac{5.376 \times 10^{10}}{s^3 + 216.7s^2 + 6.99 \times 10^7 s + 5.376 \times 10^9}. \tag{12}$$

The simulations consists in realise current tracking. Initially, the amplitude of reference current is $10A$ and it is set to $20A$ at $0.1s$. Moreover, a parametric variation over the grid impedance (1 mH + 50mΩ) is imposed at $0.15s$, changing the grid condition from strong (0.3 mH + 50mΩ) to weak (1.3 mH + 100 mΩ) condition. The reference model was chosen to have unit gain in stationary regime and it is identical for both techniques, given as follows,

$$W_m(z) = \frac{0.343}{(z - 0.3)^3}. \tag{13}$$

The following parameters, set to presented fast reference tracking, for controller and LS algorithm, were set equal for both strategies: $\boldsymbol{P}(0) = 100\boldsymbol{I}$, $\boldsymbol{\beta} = 250$, $\kappa = 25$, $\sigma_0 = 0.1$, $M_0 = 5$ and $m^2(0) = 1$. Moreover, all parameters of $\boldsymbol{\zeta}$ and $\boldsymbol{\omega}$ were initialised as zero. In the next subsections the controllers design and simulation results of each approach are presented and posteriorly discussed.

4.1 State Feedback-based RMRAC

As was aforementioned, for State Feedback-based RMRAC there are no internal filters to be designed, once they will be the own plant states. The $\boldsymbol{\omega}$ and $\boldsymbol{\theta}$ vectors are defined as follows,

$$\boldsymbol{\omega}^T(k) = [\ i_c(k)\ V_c(k)\ i_g(k)\ r(k)\ V_s(k)\ V_c(k)\ ],$$
$$\boldsymbol{\theta}^T(k) = [\ \theta_1(k)\ \theta_2(k)\ \theta_y(k)\ \theta_r(k)\ \theta_s(k)\ \theta_c(k)\ ].$$

where $i_c(k)$, $V_c(k)$ and $i_g(k)$ are the converter-side currents, capacitor voltage and grid-injected currents. Also, each parameter of $\boldsymbol{\theta}$ vector is associated to its respective parameter on $\boldsymbol{\omega}$ vector.

The initial gains $\boldsymbol{\theta}(0)$, in α and β, were set as follows,

$$\boldsymbol{\theta}_{\alpha}(0) = \begin{bmatrix} -1.7069385 \\ 0.61377239 \\ -2.3488686 \\ 0.091700301 \\ 0.59846705 \\ 0.12029804 \end{bmatrix} \quad , \quad \boldsymbol{\theta}_{\beta}(0) = \begin{bmatrix} -1.1043382 \\ 0.88677412 \\ -1.2556903 \\ 0.025422245 \\ -0.04700271 \\ 0.15242799 \end{bmatrix} .$$

Note that these gains were not chosen randomly. They were chosen taking the final values of gains provided from a previous simulation, where current reference amplitude was $10A$, during $2s$, and no parametric variation were imposed to the grid. It is not necessary initialise RMRAC gains so close to optimal gains as was made, however, as closest it be, less overshoot the system response will present. Figure 1 shows grid-injected currents, tracking their references on $\alpha\beta$ coordinates, followed their tracking errors in Figure 2.

Figure 1: Grid-side currents in $\alpha\beta$ coordinates

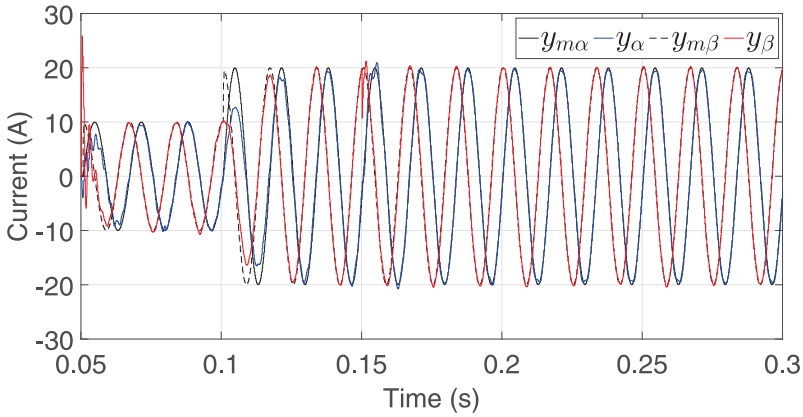

Source: From author (2021)

As can be observed, this control technique deal well with currents tracking and presented good robustness characteristics in regarding to grid impedance variation. It also rejects the exogenous disturbance properly. Besides, the great tracking error occurred on initial transitory, while gains were readapting. In steady-state the error tends to small values, however they do not achieve zero, once that was considered the switching dynamics of converter. The $\boldsymbol{\theta}(k)$ gains convergence are shown in Figure 3 and Figure 4, for α and β coordinates, as well as, covariance matrix convergence, in Figures 5 and 6, respectively.

Figure 2: Tracking error in $\alpha\beta$ coordinates

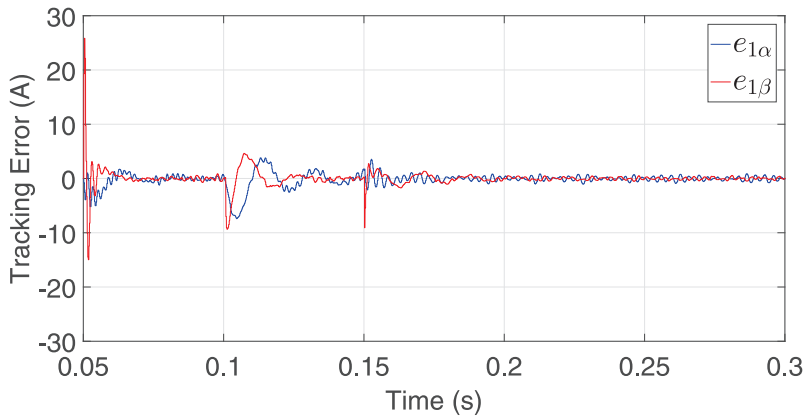

Source: From author (2021)

Figure 3: Gains in α

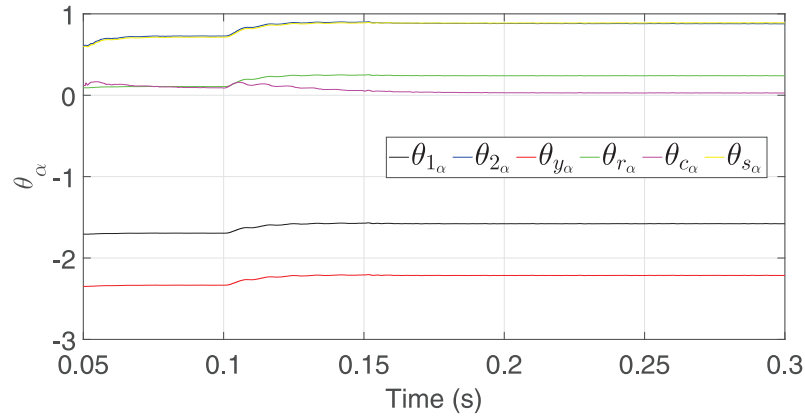

Source: From author (2021)

Figure 4: Gains in β

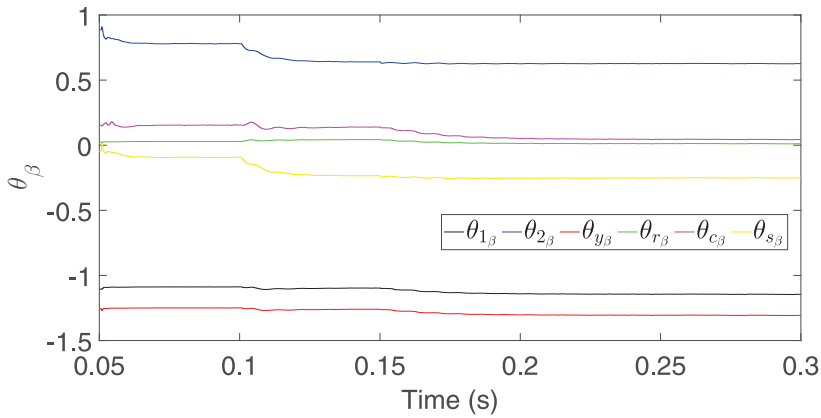

Source: From author (2021)

Figure 5: Covariance matrix in α

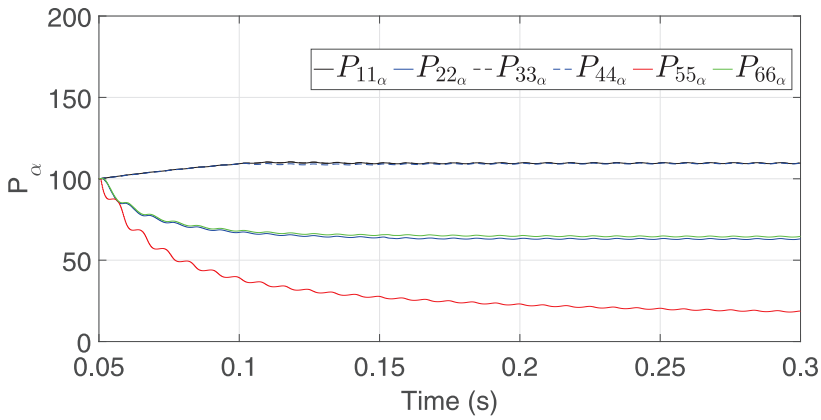

Source: From author (2021)

Figure 6: Covariance matrix in β

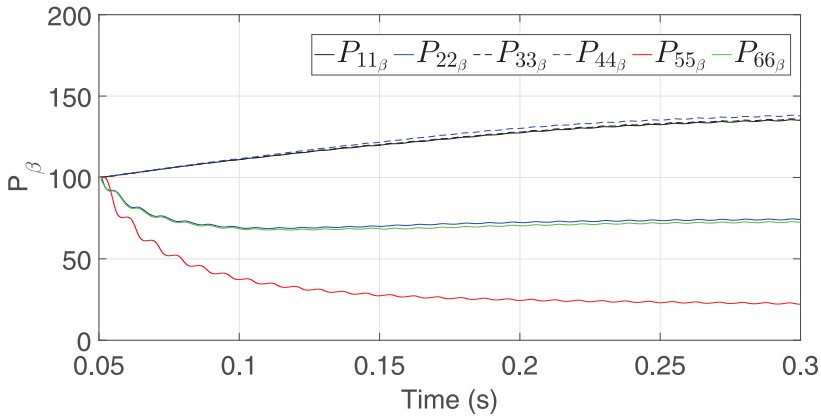

Source: From author (2021)

As can be observed, the gains adapted fast to maintain the system stable and regulating the grid injected currents. Naturally, when reference amplitude is changed, they need to readapt to the new operating point, as well as when grid condition changes. Finally, in Figure 7 the control actions are presented, where the range of required voltage to synthesise them are feasible for experimental applications.

4.2 Output Feedback-based RMRAC

In this approach there are internal filters, designed as $\boldsymbol{F} = 1000\boldsymbol{I}$ and $\boldsymbol{q} = [1000\ 0]^T$. The $\boldsymbol{\omega}$ and $\boldsymbol{\theta}$ vectors are gives as follows,

$$\boldsymbol{\omega}^T(k) = [\omega_{11}(k)\ \omega_{12}(k)\ \omega_{21}(k)\ \omega_{22}(k)\ y(k)r(k)\ V_s(k)\ V_c(k)],$$
$$\boldsymbol{\theta}^T(k) = [\theta_{11}(k)\ \theta_{12}(k)\ \theta_{21}(k)\ \theta_{22}(k)\ \theta_y(k)\theta_r(k)\ \theta_s(k)\ \theta_c(k)].$$

Figure 7: Control actions in $\alpha\beta$

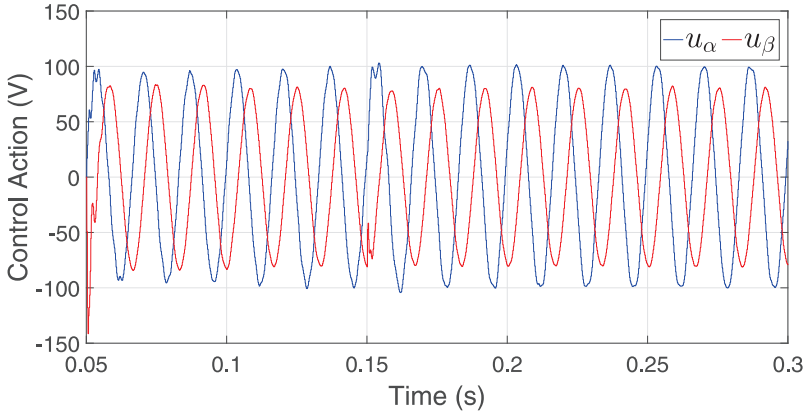

Source: From author (2021)

To be fair, the same procedure were realised to settle on the initial gains $\boldsymbol{\theta}(0)$, in α and β. It was defined as follows,

$$\boldsymbol{\theta}_\alpha(0) = \begin{bmatrix} -2.3075082 \\ 0 \\ -0.65603852 \\ 0 \\ -1.0379406 \\ 0.80786741 \\ 3.3076313 \\ -0.36709696 \end{bmatrix} \quad , \quad \boldsymbol{\theta}_\beta(0) = \begin{bmatrix} -0.84257501 \\ 0 \\ -0.32428530 \\ 0 \\ -0.83423382 \\ 0.25670955 \\ 1.5830313 \\ -0.11256287 \end{bmatrix} .$$

Figure 8 shows grid-side currents tracking in $\alpha\beta$ coordinates, followed their tracking errors in Figure 9.

In general, the controller performance is similar. However, it can be seen an more expressive tracking error on transitory regimes. In steady-state, the tracking error can be considered equivalent, as well as initial transitory error, due to gains adaptation. The $\boldsymbol{\theta}(k)$ gains convergence are shown in Figure 10 and Figure 11, for α and β coordinates, as well as , covariance matrix convergence, in Figure 12 and 13, respectively.

Again, the gains present greater adaption on transient regimes and converged on steady state, maintaining fast current tracking, robustness to the grid uncertainties and rejecting properly the exogenous disturbance. Also, the covariance matrices updating to maintain the gains converging at each transient regime.

Figure 8: Grid-side currents in $\alpha\beta$ coordinates

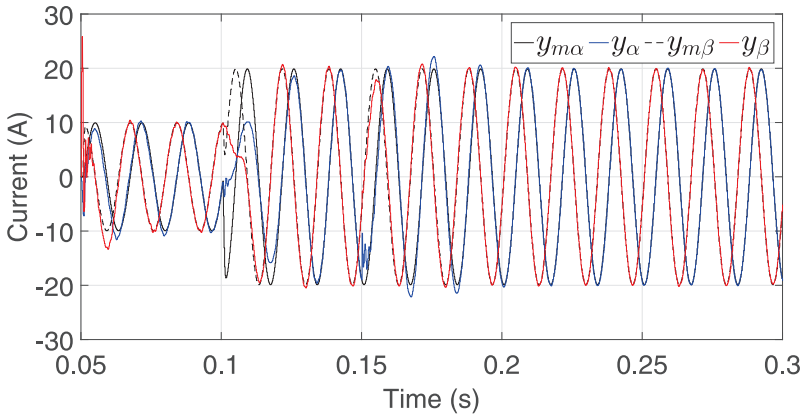

Source: From author (2021)

Figure 9: Tracking error in $\alpha\beta$ coordinates

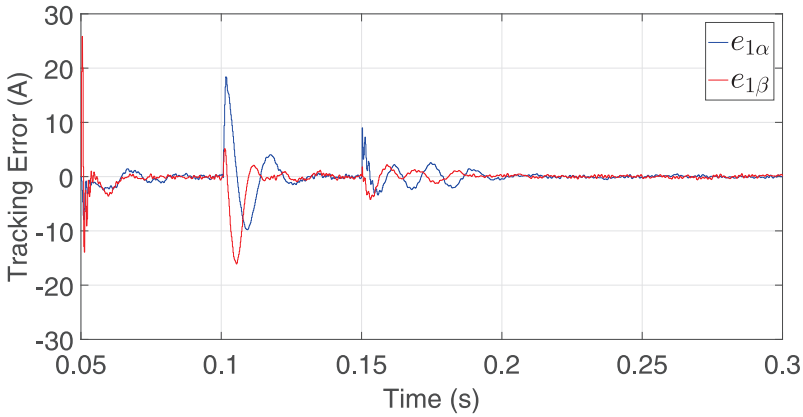

Source: From author (2021)

Figure 10: Gains in α

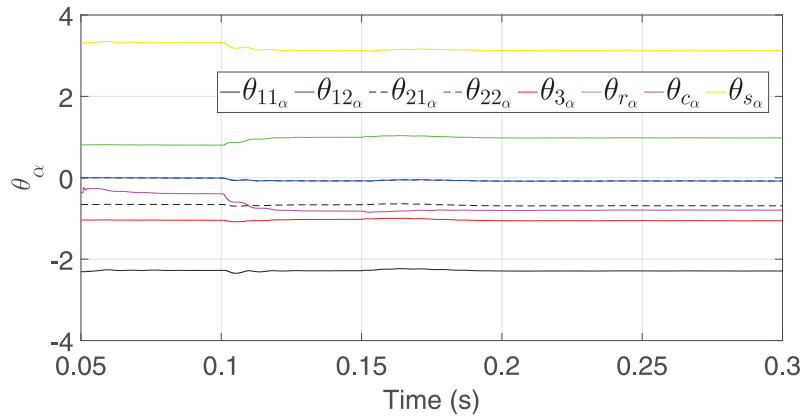

Source: From author (2021)

DOI: 10.21575/25254782rmetg2021vol6n21533

Figure 11: Gains in β

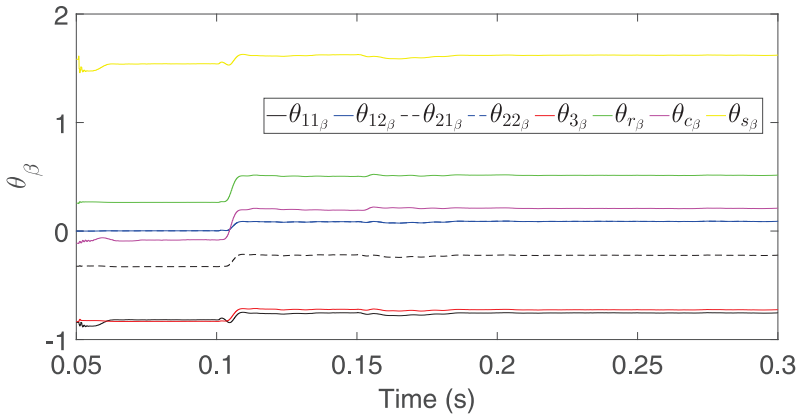

Source: From author (2021)

Figure 12: Covariance matrix in α

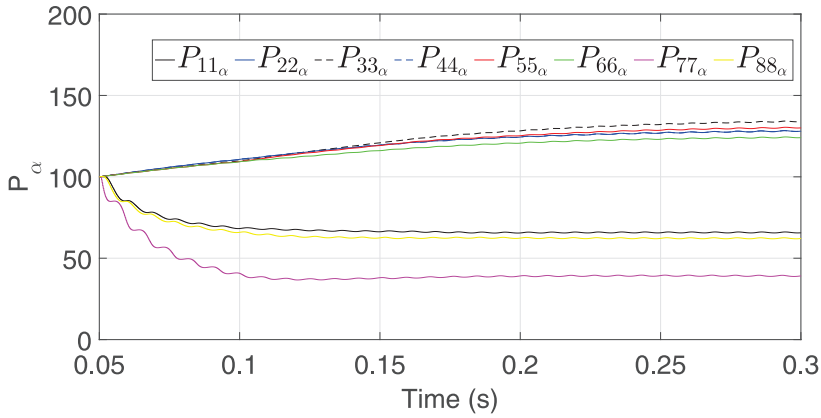

Source: From author (2021)

Figure 13: Covariance matrix in β

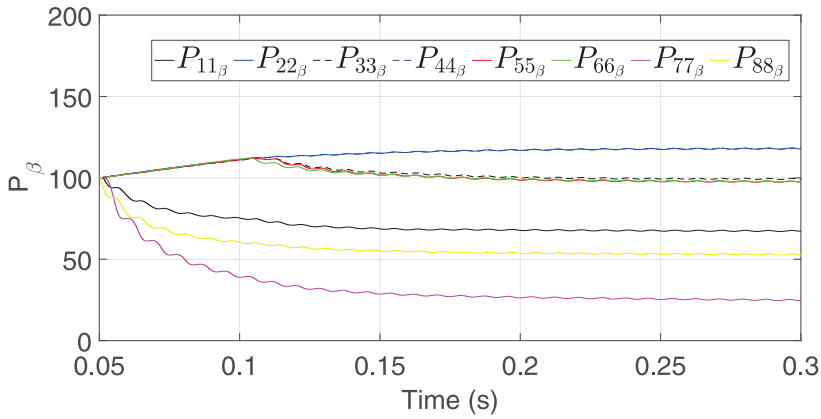

Source: From author (2021)

Finally, on Figure 14, the control actions are presented, which is similar to the State Feedback-based RMRAC.

Figure 14: Control actions in $\alpha\beta$

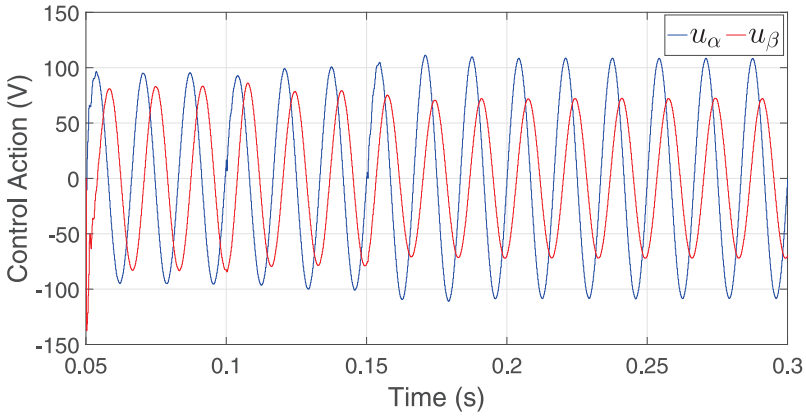

Source: From author (2021)

As can be observed, the control action are stronger when the gains are converging. Once the transient regime ends, the control actions remains in a well-defined range. This range, as well as State Feedback-based RMRAC is feasible for experimental systems.

4.3 Controllers Comparison

In regarding to the controller performance, both controllers presented satisfactory current tracking response, where the output reference model were fast tracked, with short transient regime and overshoot do not achieved great values, once gains are properly initialised. However, State Feedback-based RMRAC presented slightly better performance. The mean tracking error of Output Feedback-based RMRAC were $|\bar{e}|_{1\alpha} = 1.0448938A$, $|\bar{e}|_{1\beta} = 0.82417414A$, while for State Feedback-based RMRAC were $|\bar{e}|_{1\alpha} = 0.77860499A$, $|\bar{e}|_{1\beta} = 0.67630686A$. By the other hand, THD and maximum overshoot for both control approaches were identical: $THD_\alpha = 0.039268169\%$, $THD_\beta = 0.025991137\%$ and $25.84235A$, respectively. Thereby, both controllers are feasible for control loop of grid-injected currents of a grid-tied power converter with LCL filter.

Then, the rules for choosing the suitable control technique is availability of current and voltage sensors and microprocessor capacity. To implement the State Feedback-based RMRAC, there is the need having 9 sensors (3 sensors for capacitor voltage, 3 sensors for grid-injected currents and 3 sensor for converter-side currents), besides the sensors required on both techniques, which are used to measure voltages on

PCC, required to synchronise converter and the grid and a sensor to measure DC voltage, once it is commonly controlled. By the other hand, the Output Feedback-based RMRAC requires a reduced set of sensors, to measure grid-injected currents. It implies 6 sensors less than State Feedback-based RMRAC. However, it requires more processing capacity from microcontroller to execute it, due to the presence of internal auxiliary filters, which implies on more gain to be adapted continuously. It is important take it into account, once LS algorithm already impose a considerable computational burden.

5 Conclusion

In this work, a performance comparison of two LS-based RMRAC for grid-tied power converters with LCL filter are presented. The first technique is based on State Feedback-based RMRAC, which requires sensors to measure converter-side currents, capacitor voltages and grid-injected currents to fed back the control loop. By the other hand, the second control technique is based on Output Feedback-based RMRAC, which requires a reduced set of sensor, to measure grid-injected currents. Both controllers were designed using a modified LS algorithm to update the controller gains and simulated considerating delay implementation.

The presented comparison take into account THD, mean of absolute tracking error and maximum overshoot. To be fair, the condition for both simulation were the same, as well as, the adaption law and methodology to initialise the controller gains. In general, both controllers assure stability and robustness to the application, however, the State Feedback-based RMRAC approach presented a slightly better performance than State Feedback-based RMRAC approach by means of absolute tracking error. As main drawback, this approach requires more sensors for experimental implementation than other control approach. Then, the rule to choose the RMRAC approach can be defined as a relation of use more sensors or deal with a algorithm with more computational burden.

References

AMARAL, C. T.; LIMA, J. T. G. P.; GUEDES, R. da S. Reavaliação da valoração econômica dos recursos ambientais impactados com a usina hidrelétrica de santo antônio. ***InterEspaço: Revista de Geografia e Interdisciplinaridade***, v. 2, n. 6, p. 235–252, 2017.

BENRABAH, A.; XU, D.; GAO, Z. Active disturbance rejection control of lcl-filtered grid-connected inverter using padé approximation. ***IEEE Transactions on Industry Applications***, IEEE, v. 54, n. 6, p. 6179–6189, 2018.

BOSCH, S.; STAIGER, J.; STEINHART, H. Predictive current control for an active power filter with lcl-filter. ***IEEE Transactions on Industrial Electronics***, IEEE, v. 65, n. 6, p. 4943–4952, 2017.

BRITO, B. D. M. d.; AGUIAR, M. A. R. Sustentabilidade ou impacto ambiental: Um estudo de caso sobre o projeto usina hidrelétrica do bem querer em caracaraí-roraima. ***Revista Multidisciplinar Pey Këyo Científico***, v. 4, n. 3, p. 1–13, 2019.

BROEER, T. et al. A demand response system for wind power integration: Greenhouse gas mitigation and reduction of generator cycling. ***CSEE Journal of Power and Energy Systems***, CSEE, v. 4, n. 2, p. 121–129, 2018.

BROUWER, A. S. et al. Operational flexibility and economics of power plants in future low-carbon power systems. ***Applied Energy***, Elsevier, v. 156, p. 107–128, 2015.

CARDOSO, R. et al. Kalman filter based synchronisation methods. ***IET Generation, Transmission & Distribution***, IET, v. 2, n. 4, p. 542–555, 2008.

DUESTERHOEFT, W.; SCHULZ, M. W.; CLARKE, E. Determination of instantaneous currents and voltages by means of alpha, beta, and zero components. ***Transactions of the American Institute of Electrical Engineers***, IEEE, v. 70, n. 2, p. 1248–1255, 1951.

EVALD, P. J. D. d. O.; TAMBARA, R. V.; GRÜNDLING, H. A. A discrete-time robust mrac applied on grid-side current control of a grid-connected three-phase converter with lcl filter. ***ELECTRIMACS 2019: Selected Papers***, Springer Nature, v. 615, p. 45, 2020.

EVALD, P. J. D. O. et al. A discrete-time adaptative pi controller for grid-connected voltage source converter with lcl filter. ***Eletrônica de Potência***, Associação Brasileira de Eletrônica de Potência, v. 26, n. 1, p. 1–12, 2021.

EVALD, P. J. D. O. et al. A new discrete-time pi-rmrac for grid-side currents control of grid-tied three-phase power converter. ***International Transactions on Electrical Energy Systems***, Wiley, v. 1, n. 1, p. e12982, 2021.

EVALD, P. J. D. O.; TAMBARA, R. V.; GRÜNDLING, H. A. A direct discrete-time reduced order robust model reference adaptive control for grid-tied power converters with lcl filter. ***Eletrônica de Potência***, Associação Brasileira de Eletrônica de Potência, v. 25, n. 3, p. 361–372, 2020.

FARAKHOR, A.; ABAPOUR, M.; SABAHI, M. Design, analysis, and implementation of a multiport dc–dc converter for renewable energy applications. ***IET Power Electronics***, IET, v. 12, n. 3, p. 465–475, 2018.

FEARNSIDE, P. Gases de efeito estufa no eia-rima da hidrelétrica de belo monte. ***Novos Cadernos***, v. 14, n. 1, p. 1–16, 2011.

FLORA, L. D.; GRÜNDLING, H. A. Design of a robust model reference adaptive voltage controller for an electrodynamic shaker. ***Eletrônica de Potência***, v. 13, n. 3, p. 133–140, 2008.

GAO, C. et al. Current multi-loop control strategy for grid-connected inverter with lcl filter. In: IEEE. *33rd Youth Academic Annual Conference of Chinese Association of Automation (YAC)*. [S.l.], 2018. p. 712–716.

GUAN, Y. et al. The dual-current control strategy of grid-connected inverter with lcl filter. ***IEEE Transactions on Power Electronics***, IEEE, v. 34, n. 6, p. 5940–5952, 2018.

HAN, Y. et al. Analysis and design of improved weighted average current control strategy for lcl-type grid-connected inverters. ***IEEE Transactions on Energy Conversion***, IEEE, v. 32, n. 3, p. 941–952, 2017.

HE, J. et al. Deadbeat weighted average current control with corrective feed-forward compensation for microgrid converters with nonstandard lcl filter. ***IEEE Transactions on Power Electronics***, IEEE, v. 32, n. 4, p. 2661–2674, 2016.

HUERTA, F. et al. Lqg servo controller for the current control of lcl grid-connected voltage-source converters. ***IEEE Transactions on Industrial Electronics***, IEEE, v. 59, n. 11, p. 4272–4284, 2011.

IOANNOU, P.; TSAKALIS, K. A robust direct adaptive controller. ***IEEE Transactions on Automatic Control***, IEEE, v. 31, n. 11, p. 1033–1043, 1986.

IOANNOU, P. A.; SUN, J. ***Robust adaptive control***. [S.l.]: Courier Corporation, 2012.

KANTAR, E.; HAVA, A. M. Optimal design of grid-connected voltage-source converters considering cost and operating factors. ***IEEE Transactions on Industrial Electronics***, IEEE, v. 63, n. 9, p. 5336–5347, 2016.

KIPKE, V.; CHHOR, J.; SOURKOUNIS, C. Actively damped pi-based control design of grid-connected three-level vsc with lcl filter. In: IEEE. *44th Annual Conference of the IEEE Industrial Electronics Society (IECON)*. [S.l.], 2018. p. 973–978.

LEITNER, S. et al. Internal model-based active resonance damping current control of a grid-connected voltage-sourced converter with an lcl filter. ***IEEE Transactions on Power Systems***, IEEE, v. 33, n. 6, p. 6025–6036, 2018.

LIMA, D. M. et al. Kalman filter observers with harmonic disturbance estimation applied to a grid-connected lcl filter. In: IEEE. *13th IEEE International Conference on Industry Applications (INDUSCON)*. [S.l.], 2018. p. 730–737.

MAHMUD, R.; RAHMAN, M. A. Proportional integral resonant current controller for grid connected inverter in distributed generation system using svpwm technic. In: IEEE. *International Conference on Computer, Communication, Chemical, Material and Electronic Engineering (IC4ME2)*. [S.l.], 2018. p. 1–4.

MASSING, J. R.; PINHEIRO, H. Adaptive current control of grid-connected vsc with lcl-filters using parallel feedforward compensation. In: IEEE. *36th Annual Conference on IEEE Industrial Electronics Society (IECON)*. [S.l.], 2010. p. 3185–3191.

MASSING, J. R. et al. Adaptive current control for grid-connected converters with lcl filter. ***IEEE Transactions on Industrial Electronics***, IEEE, v. 59, n. 12, p. 4681–4693, 2011.

NOURELDEEN, O.; HAMDAN, I. Design of robust intelligent protection technique for large-scale grid-connected wind farm. ***Protection and Control of Modern Power Systems***, SpringerOpen, v. 3, n. 1, p. 17, 2018.

PINHEIRO, H. et al. Modulação space vector para inversores alimentados em tensão: uma abordagem unificada. ***Sba: Controle & Automação Sociedade Brasileira de Automatica***, SciELO Brasil, v. 16, n. 1, p. 13–24, 2005.

SILVEIRA, W. B. da et al. A new discrete-time robust adaptive predictive control-based rmrac applied to grid connected converters with lcl-filter. In: *XXIII Congresso Brasileiro de Automática (CBA)*. [S.l.: s.n.], 2016.

TAMBARA, R. V. et al. A discrete-time robust adaptive controller applied to grid-connected converters with lcl filter. ***Journal of Control, Automation and Electrical Systems***, Springer, v. 28, n. 3, p. 371–379, 2017.

TAMBARA, R. V. et al. A digital rmrac controller based on a modified rls algorithm applied to the control of the output currents of an lcl-filter connected to the grid. In: IEEE. *2013 15th European Conference on Power Electronics and Applications (EPE)*. [S.l.], 2013. p. 1–8.

VIEIRA, R. P. et al. Sliding mode controller in a multiloop framework for a grid-connected vsi with lcl filter. ***IEEE Transactions on Industrial Electronics***, IEEE, v. 65, n. 6, p. 4714–4723, 2017.

XIN, Z. et al. Mitigation of grid-current distortion for lcl-filtered voltage-source inverter with inverter-current feedback control. ***IEEE Transactions on Power Electronics***, IEEE, v. 33, n. 7, p. 6248–6261, 2017.

XU, J.; XIE, S.; TANG, T. Active damping-based control for grid-connected lcl-filtered inverter with injected grid current feedback only. ***IEEE Transactions on Industrial Electronics***, IEEE, v. 61, n. 9, p. 4746–4758, 2013.

ZHANG, X. et al. Study of a current control strategy based on multisampling for high-power grid-connected inverters with an lcl filter. ***IEEE Transactions on Power Electronics***, IEEE, v. 32, n. 7, p. 5023–5034, 2016.

ZHAO, W.; CHEN, G. Comparison of active and passive damping methods for application in high power active power filter with lcl-filter. In: IEEE. *International Conference on Sustainable Power Generation and Supply (SUPERGEN)*. [S.l.], 2009. p. 1–6.

Enviado em: 06 fev. 2021

Aceito em: 30 jul. 2021

Editores responsáveis: Bianca Neves Machado / Mateus das Neves Gomes